



# Impact of thermal annealing on wettability and antifouling characteristics of alginate poly-L-lysine polyelectrolyte multilayer films



Eleftheria Diamanti<sup>a</sup>, Nicolas Muzzio<sup>b</sup>, Danijela Gregurec<sup>a</sup>, Joseba Irigoyen<sup>a</sup>, Miguel Pasquale<sup>b</sup>, Omar Azzaroni<sup>b</sup>, Martin Brinkmann<sup>c</sup>, Sergio Enrique Moya<sup>a,\*</sup>

<sup>a</sup> Soft Matter Nanotechnology Group, CIC biomaGUNE, Paseo Miramón 182C, 20009 San Sebastián, Guipúzcoa, Spain

<sup>b</sup> Instituto de Investigaciones Físicoquímicas Teóricas y Aplicadas (INIFTA), (UNLP, CONICET), Sucursal 4, Casilla de Correo 16, 1900 La Plata, Argentina

<sup>c</sup> Experimental Physics, Saarland University, 66123 Sarbrücken, Germany

## ARTICLE INFO

### Article history:

Received 14 November 2015

Received in revised form 29 April 2016

Accepted 4 May 2016

Available online 7 May 2016

### Keywords:

Polyelectrolyte multilayers

Thermal annealing

Biopolymers

Wettability

Antifouling

## ABSTRACT

Polyelectrolyte multilayers (PEMs) of poly-L-lysine (PLL) and alginate sodium salt (Alg) are fabricated applying the layer by layer technique and annealed at a constant temperature; 37, 50 and 80 °C, for 72 h. Atomic force microscopy reveals changes in the topography of the PEM, which is changing from a fibrillar to a smooth surface. Advancing contact angle in water varies from 36° before annealing to 93°, 77° and 95° after annealing at 37, 50 and 80 °C, respectively. Surface energy changes after annealing were calculated from contact angle measurements performed with organic solvents. Quartz crystal microbalance with dissipation, contact angle and fluorescence spectroscopy measurements show a significant decrease in the adsorption of the bovine serum albumin protein to the PEMs after annealing. Changes in the physical properties of the PEMs are interpreted as a result of the reorganization of the polyelectrolytes in the PEMs from a layered structure into complexes where the interaction of polycations and polyanions is enhanced. This work proposes a simple method to endow bio-PEMs with antifouling characteristics and tune their wettability.

© 2016 Elsevier B.V. All rights reserved.

## 1. Introduction

Polyelectrolyte multilayers (PEMs) fabricated by means of the Layer by Layer (LbL) technique have found multiple applications in the last years for surface engineering and device fabrication [1–3]. PEMs have potential applications in diverse areas such as optoelectronics, nanofiltration and tissue engineering [4–8]. Recently, PEMs have attracted attention as antifouling coatings, as they can be easily assembled on almost any charged surface and the stepwise assembly of polyelectrolytes allows for a precise control of composition of the multilayers in the vertical plane combining different polyelectrolytes and nanomaterials, with synergic antifouling effects. In this regards several interesting strategies have been followed i.e. the use of perfluorinated PEG co-polymers as layer constituents, the control of the surface charge density or the use of a sacrificial top layer that can be removed together with the foulant and later reassembled [9–12].

PEMs are assembled by the alternating deposition of polycations and polyanions on top of charged surfaces, based on attractive electrostatic interactions and entropy considerations, since counterions are released during the PEM assembly [13–15]. The LbL process can be considered as a special case of polycation/polyanion complex formation. The layered structure of the film is a consequence of the step-wise assembly of polycations and polyanions. However, the layers are not fully stratified, as there is a certain degree of interdigitation among them. One layer in PEMs can be sensed up to 4 layers below [16]. Interdigitation is partially a consequence of the presence of free space within the film, which is filled by the following depositing layers [17].

PEMs are very stable; they are not easily removed, unless at least one of the polyelectrolytes is weak and loses charges by changing the pH, or there is a specific ion or surfactant interacting with the monomers that can weaken the electrostatic attraction between oppositely charged polyelectrolytes [18,19]. Only at very high ionic strength the films can be partially erased [20]. Despite PEM stability, the layered arrangement of the polyelectrolyte is not the energetically optimal. From an intuitive point of view the best arrangement of the oppositely charged polyelectrolytes would not

\* Corresponding author.

E-mail address: [smoya@cicbiomagune.es](mailto:smoya@cicbiomagune.es) (S.E. Moya).

be as separated layers but as complexes, where there is a maximal compensation of the negative and positive charges. In a complex the oppositely charged polyelectrolytes will be closer than in the LbL assembly. However, a reorganization of the PEMs into complexes, with the disappearance of the characteristic stratified structure could compromise the stability of the PEM itself.

Thermal annealing, exposing the PEMs to heat for a defined period of time, gives the polyelectrolyte molecules the energy to rearrange in the films and find more convenient conformations. It has been shown that annealing to capsules of PDADMAC/PSS leads to the rearrangement of the polymers with a consequent loss of internal volume and increase of the layer thickness. This phenomenon occurs only when PDADMAC is the last layer [21–24]. Glinel et al. show the impact of annealing on the responsive behavior of polyelectrolyte films in relation with changes on the architecture of the multilayers [25]. Besides these works there are no other reported examples related to the thermal annealing of PEMs. In this work we study the effect of thermal annealing on PEMs constructed upon two biopolymers that have been extensively used for biomedical applications as they provide enhanced surface biocompatibility; these are the positively charged poly-L-lysine (PLL) and the negatively charged alginic acid sodium salt (Alg) [26–30]. We will demonstrate that by applying annealing on these films their wetting properties will dramatically change with variations in the contact angle in water of 60°, from highly hydrophilic to hydrophobic. This variation in wetting behavior is a consequence of the rearrangement of the polymer chains, which could be visualized by Atomic Force Microscopy (AFM) [31,32]. Thermal annealing of PLL/Alg multilayers has also a clear effect on the interaction of the PEMs with proteins, decreasing protein deposition while increasing the antifouling character of the PEMs. The use of annealing at different temperatures to decrease protein deposition provides a simple procedure to tune the antifouling characteristics of surfaces without altering the chemistry of the multilayers and employing commercial and biocompatible polymers, which are amenable with biomedical applications, where limited protein deposition on surfaces may be required.

## 2. Material and methods

Poly-L-lysine solution 0.1% (w/v) in H<sub>2</sub>O (PLL, Mw 150–300 kDa), bovine serum albumin hydrolyzed powder, pH 7 ≥98% (BSA, Mw ~66 kDa), was obtained from Sigma-Aldrich. Alginic acid sodium salt (Alg, Mw 10–600 kDa) was acquired from Acros Organics. Fluorescent label ATTO 488 NHS-ester (1 mg) was purchased from ATTO – TEC – Fluorescent Labels and Dyes. Disposable PD-10 desalting columns filled with Sephadex® G-25 gel filtration medium were purchased from GE Healthcare Life Sciences. SiO<sub>2</sub> particles with a diameter of 3 μm were purchased from Attendbio.

Sodium chloride (NaCl), phosphate buffer saline (PBS), sodium bicarbonate (NaHCO<sub>3</sub>), sodium hydroxide (NaOH), (4-(2-hydroxyethyl)-1-piperazineethanesulfonic acid) (Hepes) dimethyl sulfoxide (DMSO) solvent and ethylene glycol (EG) was purchased from Sigma-Aldrich.

### 2.1. Build up of polyelectrolyte multilayer films

Each polyelectrolyte was dissolved in 10 mM Hepes/150 mM NaCl buffer (pH 7.4) at a final concentration 1 mg ml<sup>-1</sup>. Following the LbL technique 15 layers of PLL/Alg with PLL as the outermost layer; (PLL/Alg)<sub>7,5</sub>, were coated on top of negatively charged surfaces. The surfaces employed for the assembly varied according to the requirements of each experimental configuration. Samples were incubated for 10 min in each polyelectrolyte solution. Each

step of assembly was followed by washing with Hepes/NaCl buffer for the removal of the surplus polyelectrolyte.

### 2.2. Annealing process

The annealing of the samples was conducted during 3 days in a Memmert UNE 200–300 oven with a range of temperature 5–250 °C under atmosphere conditions for three different temperatures; 37 °C, 50 °C and 80 °C. For annealing all samples was first dried in air.

### 2.3. Atomic force microscopy

Structural details of the PLL/Alg films were investigated using a Nanowizard II AFM (JPK, Berlin, Germany). Images were acquired on dry samples, scanning in air. Prior to imaging polyelectrolyte films were washed with nanopure water and left to dry at room temperature. TESP-V2 cantilever (Bruker, AFM Probes) with a nominal spring constant of 40 N/m was used for imaging in intermittent mode. The resonant frequency was in the range of 280–320 kHz. The root mean square (RMS) roughness is calculated as the average of RMS line profiles across vertical and horizontal direction of the AFM images using Gwyddion software.

### 2.4. Contact angle measurements

The wetting properties of the PEM film were characterized before and after the annealing in a DSA 100 contact angle measuring system with a DSA 100 control from the Kruss Company at room temperature (20 °C) and ambient atmospheric conditions. During the measurement, the liquid drops remain attached to the steel tip with outer diameter,  $d = 0.5$  mm. Still images of a 3 μL drop with 500 μL min<sup>-1</sup> velocity were captured after the liquid volume was slowly inflated or deflated until the contact line moved gradually outward or inward, respectively. Drop profiles were recorded and fitted with the included software package (DSA 3). Apparent contact angles of the drops for 5 repetitions of each sample were obtained with a stdev = 1.9.

Contact angle measurements were performed using different test liquids to characterize the surface energy of PEMs before and after annealing. Water, ethylene glycol (EG), and dimethylsulfoxide (DMSO) were chosen as test liquids to determine the dispersion component  $\gamma_s^D$  and the polar component  $\gamma_s^P$ , as well as the total interfacial free energy of the bare substrate,  $\gamma_s$  for each test liquid, we measure the static advancing contact angle,  $\theta_a$ , and the static receding contact angle,  $\theta_r$ .

### 2.5. Polyelectrolyte assembly on colloids

For ζ-potential measurements PEMs were assembled on top of SiO<sub>2</sub> particles (3 μm). To do so, SiO<sub>2</sub> particles were first suspended in 10 mM Hepes/150 mM NaCl (pH 7.4) buffer at 1 mg ml<sup>-1</sup>. Subsequently the particles were incubated at the polyelectrolyte solution (1 mg ml<sup>-1</sup>) for 15 min. The procedure was repeated for every layer deposition for the construction of 15 layers. In between polyelectrolyte depositions three washing steps were performed via centrifugation.

### 2.6. ζ-potential measurements

Changes on the surface charge of the PEM coated colloids were recorded using a Zetasizer (Malvern, of the UK). ζ-potential measurements were conducted in a disposable folded capillary cell at 25 °C and they were performed at a cell drive voltage of 30 V, using a monomodal analysis model. Five repetitions were conducted for

each sample. Samples were diluted in 10 mM Hepes/150 mM NaCl (pH 7.4) buffer at a final concentration  $0.1 \text{ mg ml}^{-1}$ .

### 2.7. QCM-D measurements

The assembly of the PLL/Alg PEM and the deposition of BSA protein before and after annealing were monitored via the QCM-D, Q-Sense E4 system. The coating of the PEM film was conducted on  $\text{SiO}_2$  (50 nm) coated quartz crystals (5 MHz, Q-Sense). PE solutions were injected in the 4-sensor chamber with the help of a peristaltic pump and left under incubation for 10 min. After stabilization of the frequency another 10 min rinsing with 10 mM Hepes/150 mM NaCl buffer (pH 7.4) was followed. Experiments were conducted at  $23^\circ\text{C}$ . For the deposition of the protein BSA was dissolved at  $1 \text{ mg ml}^{-1}$  concentration in Hepes/NaCl buffer.

### 2.8. Fluorescence spectroscopy measurements

The adsorption of labeled BSA on PEMs was quantified using a Fluorolog<sup>®</sup> – HORIBA JOBIN YVON fluorescence spectrometer. Protein labeling was performed using amine reactive ATTO 488-Labels (NHS-Esters). The protocol used for the labeling of the BSA was obtained from ATTO-TEC. Measurements were done at emission spectral acquisition configuration, excitation was set at a wavelength of 488 nm (1 nm slit width) and the emission wavelength range was set between 510 and 700 nm (1 nm slit width). For the fluorescence measurements the PLL/Alg PEM film was deposited, following the procedure described above, on top of quartz microscope slides ( $25 \text{ mm} \times 25 \text{ mm} \times 1 \text{ mm}$ ) from UQG Optics. The ATTO 488 labeled BSA with a  $1 \text{ mg ml}^{-1}$  concentration was deposited onto the PEM films before and after annealing.

## 3. Results and discussion

### 3.1. Effect of annealing in PLL/Alg PEMs

The assembly of the PLL/Alg PEM was first followed by means of QCM-D to demonstrate the growth of the PEM upon each PE layer

deposition (Fig. 1). The continuous stepwise decrease in frequency ( $\Delta f = 524 \text{ Hz}$ ) proves the deposition of the 15 polyelectrolyte layers.

Once the multilayer was build up the films were annealed at  $37^\circ\text{C}$ ,  $50^\circ\text{C}$  and  $80^\circ\text{C}$  for 72 h as described in the experimental part.

AFM imaging was performed on the PEMs to visualize the impact of the annealing on the surface morphology. The topography and roughness of the film as assembled, without thermal annealing is displayed in Fig. 2a. The PLL/Alg PEMs display a non-homogeneous porous morphology consisted of a fibrillar network. The highest features of the network display a height up to  $\sim 150 \text{ nm}$  as seen from the roughness profile, with free space between the polymer fibers of  $1\text{--}2 \mu\text{m}$  on average.

It is worth noting that below the top fibrillar structures there is more polymeric material, assembled into fibrillar networks as well. This can be seen in the last  $5 \mu\text{m}$  of the roughness profile (bottom panel of Fig. 2a), where the substrate cannot be visualized between the highest peaks, although there are observed peaks of lower heights, reaching up to  $40 \text{ nm}$ . PEMs roughness (RMS) of  $38.2 \pm 8.3 \text{ nm}$  was calculated from the AFM images. The glass substrate underneath the PEM displays a smoother profile; for glass the roughness is in the range of  $0.5\text{--}2 \text{ nm}$  [33]. The influence of the temperature on the structural reorganization of the PEMs is shown in Fig. 2b. The PEM has been annealed at  $37^\circ\text{C}$  and displays a smoother topography. The morphology does not show any more a complete network-like organization. Instead, we observe the presence of grains across the surface, with heights of  $5\text{--}10 \text{ nm}$ . In the bottom panel of Fig. 2b, in the roughness profile, we can observe two peaks with heights of  $\sim 35 \text{ nm}$ . These peaks correspond to the features from the upper image in lighter colours, corresponding to higher values in the colour scale. These are appearing as isolated networks when compared to the ones in Fig. 2a where a network covers the whole surface. RMS decreases concomitantly to  $4.9 \pm 1.7 \text{ nm}$ . When the PEM is annealed at  $80^\circ\text{C}$ , the AFM imaging shown in Fig. 2c, reveals that the surface displays a morphology with fewer grain-like structures than at  $37^\circ\text{C}$ , and the polymer network is no longer observed. RMS, however, increases to  $8.7 \pm 5.8 \text{ nm}$  for the PEM annealed at  $80^\circ\text{C}$ , this value is slightly higher than for the PEM annealed at  $37^\circ\text{C}$  but still smaller than for the non annealed

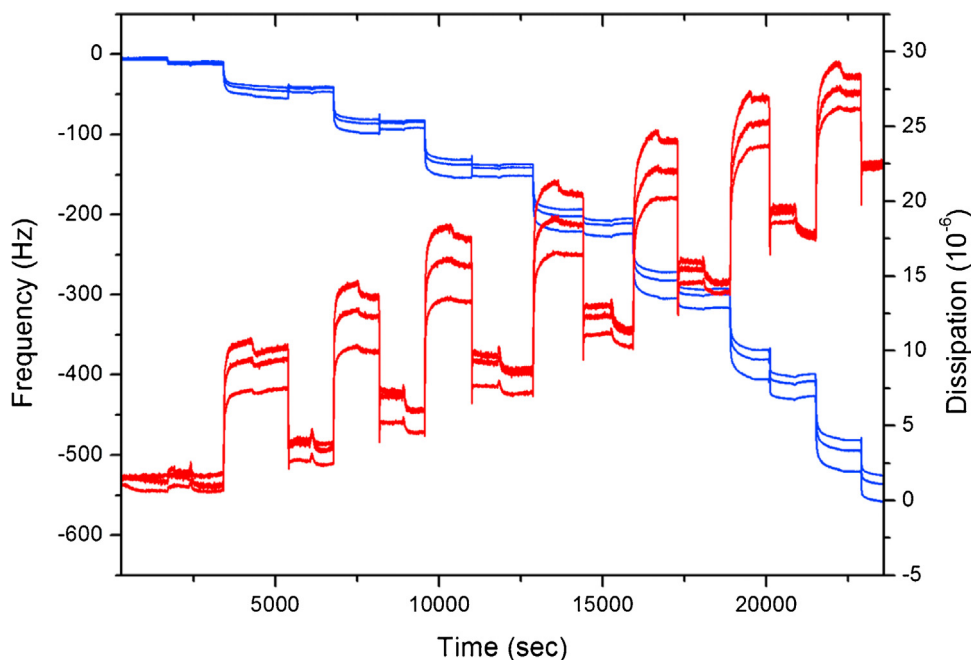
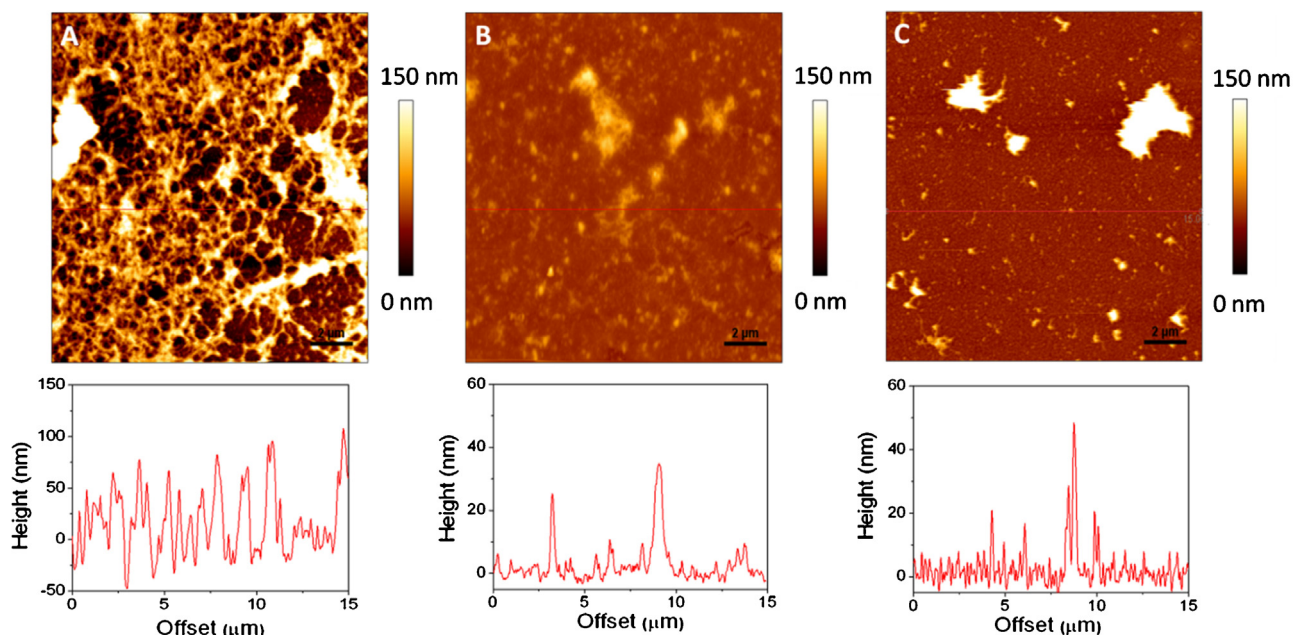


Fig. 1. QCM-D curves representing changes in frequency (in red) and dissipation (in blue) during the assembly of 15 layers of PLL/Alg. (1.5-column image). (For interpretation of the references to colour in this figure legend, the reader is referred to the web version of this article.)



**Fig. 2.** AFM images ( $15 \times 15 \mu\text{m}$ ) acquired on dry (PLL/Alg) $_{7.5}$  multilayers (a) without annealing, (b) after annealing at  $37^\circ\text{C}$  and (c) after annealing at  $80^\circ\text{C}$ . Bottom panels display roughness profiles taken as crosssections of the above images. (2-column image).

samples. AFM clearly shows that the polyelectrolyte chains reorganize when they are annealed at  $37^\circ\text{C}$  and higher temperatures. The fact that the surface becomes smoother implies that the chains are rearranging in a more compact structure and hints that the layered structure of the PLL/Alg PEM is changing, as the fibres observed in the non annealed PEM disappear progressively with the increase of temperature.

Contact angle experiments were conducted at room temperature,  $23^\circ\text{C}$ , to determine the wettability of multilayers before and after annealing at different temperatures. The mean advancing water contact angle for (PLL/Alg) $_{7.5}$  before annealing was  $36^\circ \pm 2.8^\circ$  (Fig. 3). This value corresponds to a hydrophilic surface. Both Alg and PLL are charged and considering the hydrophilic amine groups of the last PLL layer the contact angle values are reasonable. When the PEM was annealed during 72 h at  $37^\circ\text{C}$  the wetting properties of the film change drastically, giving contact angle values of  $93^\circ \pm 4.6^\circ$ . After annealing at  $50^\circ\text{C}$  and  $80^\circ\text{C}$  the contact angle changed indeed in both cases from hydrophilic to hydrophobic giving values of  $77^\circ$  and  $95^\circ$ , respectively. Surprisingly the annealing at  $50^\circ\text{C}$  caused a decrease in the contact angle in  $16^\circ$  but higher temperatures resulted again in an increase of the contact angle. These variations are indicative of a restructuring of the PEM with the temperature as the contact angle will be affected by the density of charges on the surface and the exposure of the organic backbone of the polymer chains in the PEM surface.

Table 1 provides the values of the advancing and receding contact angle for different solvents; water, EG and DMSO for the PEMs before and after annealing. The lowest contact angle was measured in DMSO, being around  $7^\circ$  (advancing) for the non annealed sample and displaying values between  $20^\circ$  and  $30^\circ$  in the case of the annealed PEMs. For EG the contact angle was  $27^\circ$  for non annealed samples and increased to values between  $28^\circ$  and  $42^\circ$  for the annealed ones. Receding contact angle could not be measured for the non annealed samples with DMSO and EG as the droplet partially absorbs on the polymer surface. There was a small hysteresis between advancing and receding contact angle values for DMSO and EG for the annealed samples. In the case of water the hysteresis was more pronounced; approximately  $10^\circ$  for the non annealed samples, and increased up to  $40^\circ$  for the sample annealed at  $80^\circ\text{C}$ .

Contact angle hysteresis on inert and rigid solids can be explained from the presence of microscopic chemical and/or topographic surface heterogeneities [34]. Both types of heterogeneities can act as ‘pinning centres to the free liquid interface and create a dense spectrum of meta-stable interfacial configurations’. Even in the limit of small interfacial velocities, these energy barriers contribute to the irreversible work necessary to displace the three phase contact line between the liquid phase, ambient air, and the solid. On the macroscopic scale of a wetting drop, this dissipation manifests in form of a history dependent static contact angle. Hence, changes of the contact angle hysteresis interval  $[\theta_r, \theta_a]$  after surface treatment can also hint to a changing degree of chemical and topographic heterogeneity of a polymer surface. Despite AFM imaging of non annealed PEMs showed a more irregular surface it is likely that the annealed PEM displayed a higher heterogeneity at subnano scale, mainly related to the charged groups which would explain the large hysteresis in water and not in the organic liquids. Contact angle hysteresis on a PEM could also be an effect of the slow equilibration kinetics between the wetting liquid and polymer surface [34]. The high contact angle hysteresis of the PEM with water, in particular for the non annealed samples can be due to slow reorientations of certain moieties of the polymer chains in contact to water. Other kinetic effects are linked to a slow migration of water molecules (swelling) into the polymer network.

The advancing and receding contact angle values for the different liquids were used to calculate the interfacial tension  $\gamma_l$  of the test liquids for non annealed and annealed PEMs along with the corresponding dispersive component,  $\gamma_l^D$ , and polar component,  $\gamma_l^P$ . Both components of the interfacial energy are determined from the Owens-Wendt method [35]. Particular values of the interfacial tension and the surface energy components are taken from the book of Van Oss [36]. Following the approach of Owens and Wendt, the free energy per area  $\gamma_{ls}$ , of an interface between a liquid (l) and a substrate (s) is related to their respective interfacial tensions  $\gamma_l$  and  $\gamma_s$  by:

$$\gamma_{ls} = \gamma_l + \gamma_s - 2(\gamma_s^D \gamma_l^D)^{\frac{1}{2}} - 2(\gamma_s^P \gamma_l^P)^{\frac{1}{2}} \quad (1)$$

where, the interfacial tension of the material (i) is the sum  $\gamma_i = \gamma_i^D + \gamma_i^P$  of both components. Employing the contact angle  $\theta$  in ther-

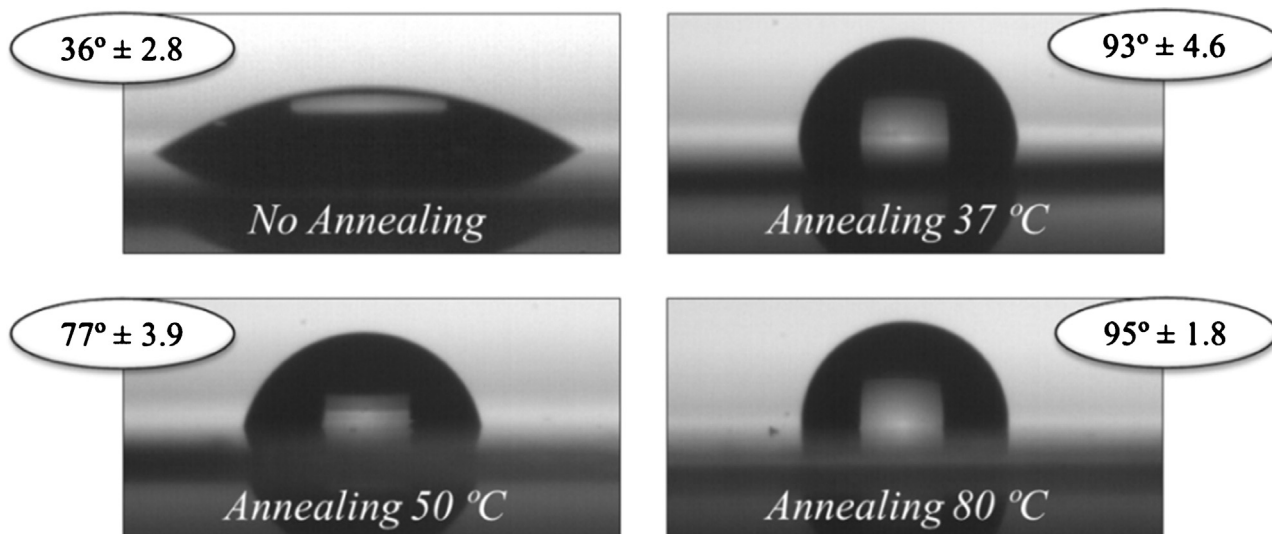


Fig. 3. Advancing water contact angle values for the (PLL/Alg)<sub>7.5</sub> films before annealing and for different annealing temperatures.

**Table 1**  
Advancing and receding contact angle values for the (PLL/Alg)<sub>7.5</sub> films before annealing and after annealing at 37, 50 and 80 °C. Contact angle values were measured with water, ethylene glycol (EG) and dimethyl sulfoxide (DMSO).

Solvents	No Annealing $T=20^{\circ}\text{C}$		Annealing at $T=37^{\circ}\text{C}$		Annealing at $T=50^{\circ}\text{C}$		Annealing at $T=80^{\circ}\text{C}$	
	$\theta_{\alpha}$	$\theta_r$	$\theta_{\alpha}$	$\theta_r$	$\theta_{\alpha}$	$\theta_r$	$\theta_{\alpha}$	$\theta_r$
DMSO	$7.3^{\circ} \pm 0.7$	–	$20.6^{\circ} \pm 1.1$	$17.6^{\circ} \pm 0.9$	$20.9^{\circ} \pm 1.8$	$19.9^{\circ} \pm 2.3$	$26.9^{\circ} \pm 2.1$	$22.6^{\circ} \pm 1.5$
EG	$27.1^{\circ} \pm 2.0$	–	$36.1^{\circ} \pm 1.4$	$28.5^{\circ} \pm 1.2$	$33.6^{\circ} \pm 1.7$	$29.5^{\circ} \pm 1.5$	$42.0^{\circ} \pm 3.6$	$39.4^{\circ} \pm 2.7$
Water	$36.0^{\circ} \pm 2.8$	$22.7^{\circ} \pm 1.3$	$93.0^{\circ} \pm 4.6$	$57.6^{\circ} \pm 2.9$	$77.0^{\circ} \pm 3.9$	$53.0^{\circ} \pm 2.0$	$95.0^{\circ} \pm 1.8$	$55.3^{\circ} \pm 2.4$

$\theta_{\alpha}$ : Static advancing contact angle.

$\theta_r$ : Static receding contact angle (2-column image).

thermodynamic equilibrium and Young's relation  $\gamma_l \cos \theta = \gamma_s - \gamma_{ls}$ , we arrive at

$$\gamma_l (1 + \cos \theta) / 2 (\gamma_l^D) = (\gamma_s^D)^{1/2} (\gamma_l^D / \gamma_l^P)^{1/2} + (\gamma_s^D)^{1/2} \quad (2)$$

being of the form  $y = mx + n$  in the variable  $x = (\gamma_l^D / \gamma_l^P)$  with a slope  $m = (\gamma_s^D)^{1/2}$  and intercept  $y_0 = (\gamma_s^D)^{1/2}$  with the ordinate. Eq. (2) allows us to determine the dispersive and the polar component of the substrate free energy by fitting the experimental data with linear relation. Experimentally, only the apparent contact angles  $\theta_a$  and  $\theta_r$  are available from measurements, and we have to make a further assumption to estimate the contact angle  $\theta$  in the thermodynamic minimum (i.e the material or Young's contact angle). In principle, it is impossible to infer the irreversible part of the work to enlarge or diminish the substrate area in contact to the wetting liquid from measurement of only  $\theta_a$ ,  $\theta_r$ , and  $\gamma_l$ . However, fundamental thermodynamic considerations demand that Young's contact angle  $\theta$  must satisfy the inequality  $\theta_r < \theta < \theta_a$ . To estimate the surface energy from the measured contact angles data we fit the advancing and receding contact angles data with Eq. (1) separately. Water is excluded because the difference between the cosines of the advancing and receding contact angles are much larger than for DMSO and EG. Here, we took the receding contact angle of DMSO and EG on the non annealed PEMs to be zero.

Fig. 4 displays an Owen-Wendt plot of the experimental data according to Eq. (2) for the PEMs without annealing and for the annealed PEMs at temperatures 37 °C, 50 °C and 80 °C. The upper and lower extremities of the error bars correspond to the data of advancing contact angles,  $\theta_a$ , and receding contact angles,  $\theta_r$ , respectively. The magnitude of the dispersion component,  $\gamma_s^D$ , and the polar component,  $\gamma_s^P$ , of the surface energy are determined from the slope and intercept, respectively, of the contact angle data

for DMSO and EG. As the contact angle hysteresis of water on the PEMs is much larger than for DMSO and EG, we excluded water for quantitative analysis.

The results of the linear interpolation, the surface energy and the respective components are summarized in Table 2. In total, the surface energy  $\gamma_s$  diminishes as the annealing temperature increases, from a value of 44.6 mJ/m<sup>2</sup> for the non annealed PEM to 38 mJ/m<sup>2</sup> after annealing at 80 °C. The surface energies after annealing at 37 °C and 50 °C were very similar and close to 40 mJ/m<sup>2</sup>.

It is interesting to look at the magnitude of the surface energy components  $\gamma_s^D$  and  $\gamma_s^P$  separately. In comparison to the non annealed sample, the polar component  $\gamma_s^P$  decreases almost to the half value after annealing at 37 °C. However, the polar component does not differ significantly from samples annealed at 37 °C and at 50 °C. Only after annealing at the highest temperature, 80 °C, the magnitude of  $\gamma_s^P$  shows a further decrease. On the other hand, the dispersion component  $\gamma_s^D$  increases gradually between annealing at 37 °C, 50 °C and 80 °C by roughly 15%.

The significant decrease of  $\gamma_s^P$  between 37 °C and 80 °C is indicative of the further compensation of the charges of PLL and Alg and would hint that the polyelectrolyte layers are reorganizing to find themselves in an energetically more favourable arrangement, where the interaction between positive and negative charges of the polyelectrolytes is maximized. The increase in  $\gamma_s^D$  in parallel is indicative of the surface becoming more hydrophobic and with a lower charge density, which is also coherent with the charge compensation. The annealing seems to induce a rearrangement of the layers into a more complex like structure where the oppositely charged Alg and PLL are closer and the charges more compensated. The results at 50 °C are more surprising. It seems that after annealing for three days at that temperature the arrangement of the chains on the surface was such that the PEMs become more

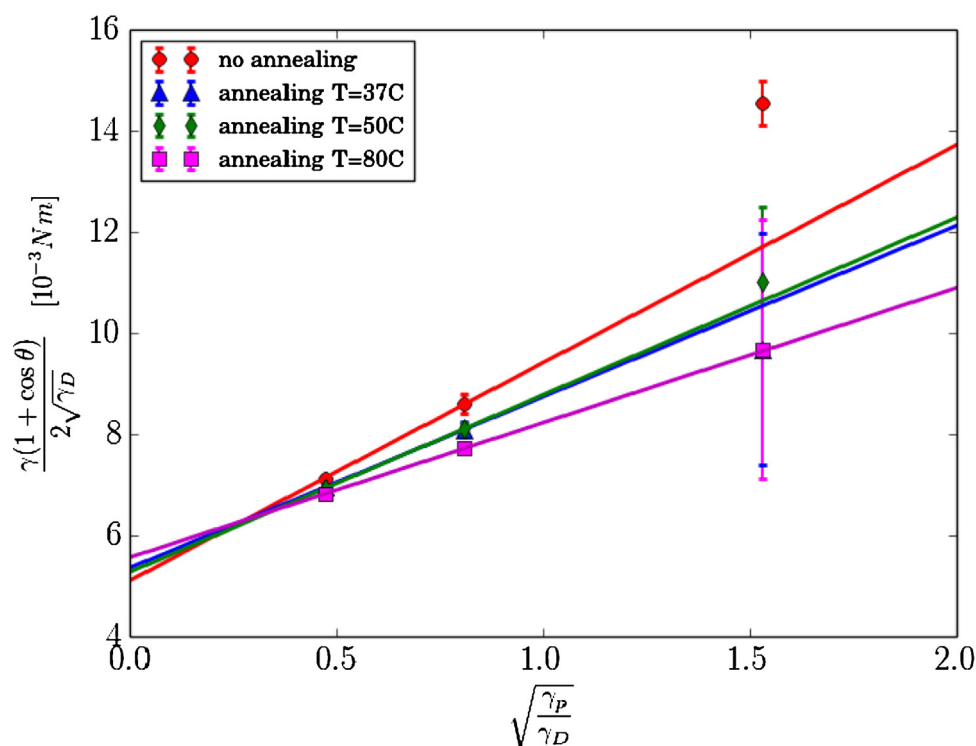


**Fig. 4.** Owens-Wendt plot to determine the polar and dispersive component of the surface energy for the multi-layer coated substrates after annealing at different temperatures. (1.5-column image).

**Table 2**

Surface energies of (PLL/Alg)<sub>5,5</sub> substrate. (1.5-column image).

Surface energy [mj/m <sup>2</sup> ]	No annealing	Annealing at T= 37 °C	Annealing at T= 50 °C	Annealing at T= 80 °C
Dispersion $\gamma_s^D$	26.5 ± 1.5	28.7 ± 1.5	27.8 ± 1.3	30.9 ± 0.5
Polar $\gamma_s^P$	18.6 ± 4.5	11.5 ± 2.5	12.3 ± 1.9	7.11 ± 0.8
Total $\gamma_s$	45.1 ± 6.0	40.2 ± 4.0	40.1 ± 3.2	38.0 ± 1.3

hydrophilic. Probably the annealing at this temperature induces a restructuring of the layers that results in a higher density of alginate on the surface. Further experiments are needed to understand this observation.

The possibility that the annealing could induce changes in the chemistry of the PEMs was also analysed. Amide bonds could be forming between the carboxylate of alginates and primary amines of PLL during the annealing. XPS measurements were performed for the PEMs before and after the annealing at all three considered temperatures. High resolution spectra of N 1s region are shown in Fig. S1. Two peaks are assigned to N–CO/C–NH<sub>2</sub> and C–NH<sub>3</sub> bonds at ~400 eV and ~401.5 eV, respectively [37]. No changes in the XPS spectra regarding the binding energies of the two species could be observed between the reference spectra of non annealed PEMs (Fig. S1a) and PEMs annealed at 37, 50 and 80 °C (Fig. S1 b–d). If there is crosslinking between the amines of PLL and the carboxylates of alginate an amide bond should be formed but this is already present in PLL and consequently there would not appear new signals. However, the ratio of the intensity of the bands of N–CO/C–NH<sub>2</sub> and C–NH<sub>3</sub> changes with the annealing. The band of N–CO/C–NH<sub>2</sub> increases in relation with the C–NH<sub>3</sub>. This could be meaning that more N–CO is being formed after the annealing, which would be the result of the crosslinking of the amines of PLL with the carboxylate groups of alginate. But at the same time the relative increase of the bands at 400 eV to the one at 401.5 eV could mean that the NH<sub>3</sub> groups are deprotonating with annealing and the relative amount of NH<sub>2</sub> increases. This would be a consequence of the dehydration of the pendant groups of PLL. When we compare the surface chem-

ical composition of the samples, the molar percentages of C, O and N (Table S1), we do not observe any significant changes between non annealed and annealed samples. The crosslinking of the PEM should result in a decrease in the O content as during the formation of an amide bond a OH group from the alginate is lost. Therefore, the absence of changes in the molar percentage of C, N, and O in the film after annealing, hint that there is no crosslinking taking place. Also, if crosslinking were taking place one would expect the PEMs to be more stable and in the case of annealing at 80 °C we observe that the film can be partially erased (Fig. 6). Therefore, despite we cannot fully disregard the possibility of crosslinking we strongly believe that the changes observed in contact angle must be associated with the electrostatic compensation of the charges of polycations and polyanions due to polyelectrolyte rearrangement.

We further investigated changes in charge density in the PEMs after annealing by  $\zeta$ -potential measurements. (PLL/Alg)<sub>7,5</sub> were assembled on colloidal particles and annealed afterwards. The annealing of the colloidal particles was also done in dry state. The particles were placed in the oven during 72 h for each annealing temperature. Finally, the annealed particles were suspended in the HEPES/NaCl solution to measure the  $\zeta$ -potential. Before annealing the  $\zeta$ -potential of the PEM was –1.3 mV and after annealing at 37 °C changed to –14.1 mV. By further increase of the temperature at 80 °C, the  $\zeta$ -potential showed a more pronounced decrease to –27 mV. The negative potential of the non annealed PEMs which is very close to zero is indicative either of the Alg chains protruding from the PEM or of the interdigitation of the PLL and Alg layers. From QCM-D measurements we know that the film grows progressively

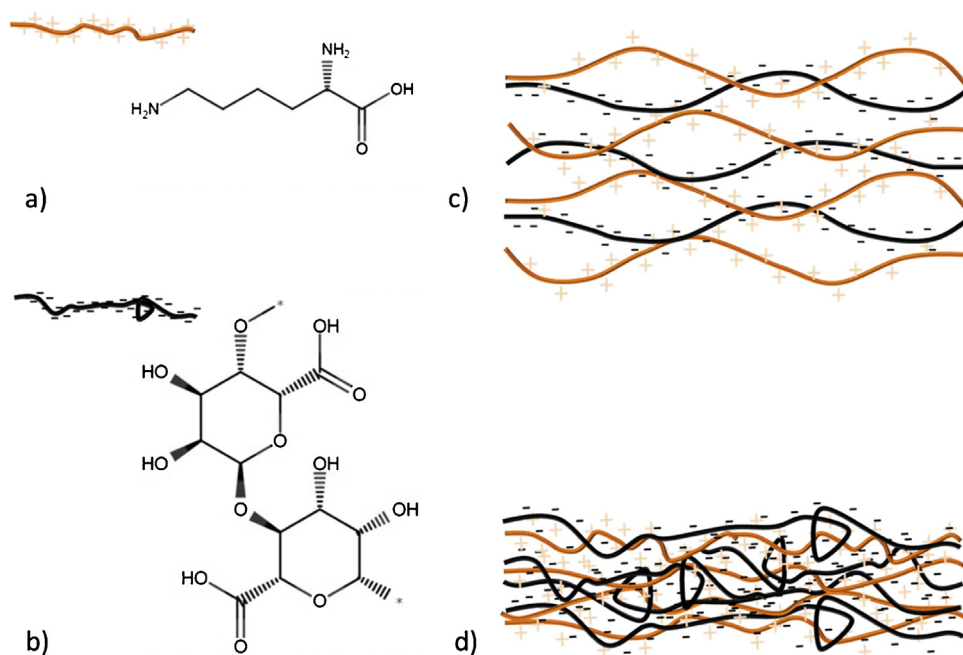


**Fig. 5.** Representation of the chemical structures of (a) poly-L-lysine and (b) alginate sodium salt. Scheme of the structure of the PLL/Alg polyelectrolyte multilayer (c) before and (d) after annealing. (1.5-column image).

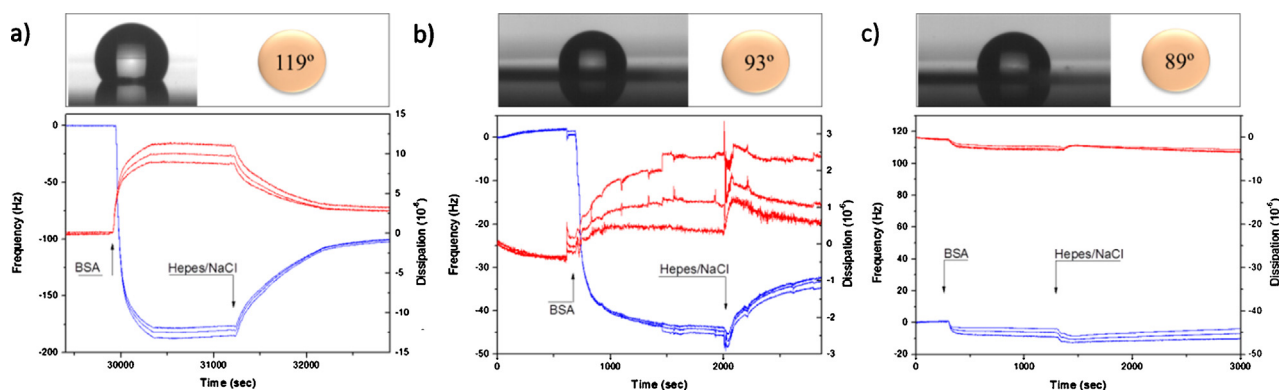


**Fig. 6.** Changes in frequency and dissipation after adsorption of BSA protein on top of (PLL/Alg)<sub>7.5</sub> coated SiO<sub>2</sub> QCM-D crystals and their corresponding contact angle data for the cases of (a) non annealed surface, (b) annealed surface at 37 °C and (c) annealed surface at 80 °C. (2-column image).

and the last layer of PLL is deposited on top of the PEM. There may also be slight differences in the layer characteristics when going from the planar PEM surfaces to a colloidal one as the assembly processes involves steps that are not included on the planar assembly in QCM-D. Nevertheless, despite the slightly negative value it is interesting to follow the evolution of the surface charge with the annealing. As the annealing temperature increased the charge became more negative. This means that either the last PLL layer is removed or most likely there is rearrangement of the Alg and PLL molecules leaving the Alg chain more exposed to the surface and probably surrounding the PLL molecules which are trapped in the Alg. The fact that the maximum molecular weight of Alginate is 600 kD while for PLL is only 300 kD could explain the excess of negative charges. As the complexes between PLL and Alg molecules are formed there is a compensation of the charges and the charge of the longer chains prevails.

The annealing process allows the polyelectrolyte to restate and reorganize to a molecular arrangement where the interaction of the oppositely charged polyelectrolytes is maximized. The  $\zeta$ -potential measurements hint to a situation where after annealing Alg charges are more presented on the surface resulting to a higher density of

negative surface charge than before the annealing. However, this does not mean that the density of hydrophilic groups is higher than before annealing, since the top layer was PLL with positively charged amines. A lower density of hydrophilic groups is hinted by the changes in the polar component of the surface energy, which decreases significantly with the annealing at 80 °C. It is important to take into account that the annealing take place in dry conditions, thus a possible driving force for the process would be the decrease in the PEM surface/air interfacial energy, thus an enhanced amount of hydrophobic groups are expected to be found at the interface, as it has been reported [13]. This would cause a decrease in the density of hydrophilic groups on the surface. AFM shows clearly the reorganization of the surface under the annealing process. The surface roughness of the PEM gets smoother as the annealing temperature increases. This probably indicates that the grains intermix as complexes are being formed.

A scheme of the proposed rearrangement of the PEM after annealing is shown in Fig. 5. In the scheme we have sketched the layered structure of the PEMs and the disappearance of this structure after heating, resulting in the formation of complexes of Alg and PLL chains.

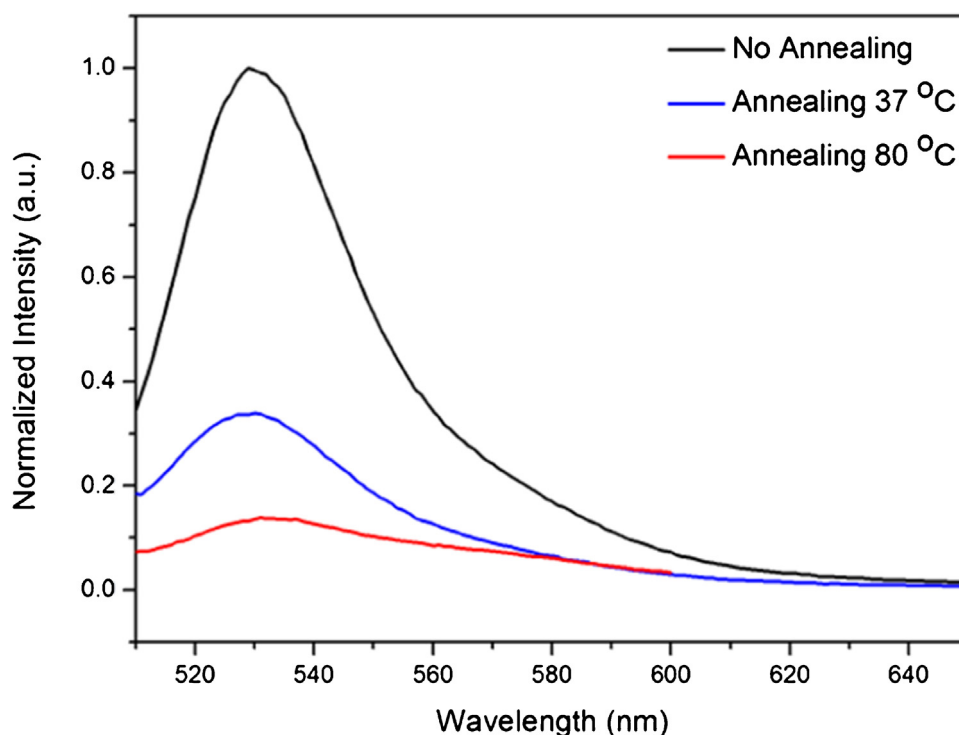


Fig. 7. Fluorescence spectroscopy spectra after adsorption of labelled BSA onto the (PLL/Alg)<sub>7.5</sub> films before and after annealing at 37 and 80 °C. (1.5-column image).

### 3.2. Interaction of PEMs with proteins

In several situations the interaction of PEMs with proteins is of critical importance. Charged proteins normally interact with PEMs electrostatically so their deposition depends on the charge of both PEM and protein. We studied the interaction of the bovine serum albumin (BSA) protein, and the film before and after annealing. QCM-D experiments were conducted to monitor the adsorption of the BSA on the PEM. PEMs deposited on the quartz crystals were annealed with the same procedure used for the films assembled on glass surfaces, placed back in the QCM-D chamber and rehydrated with the buffer prior to exposure to the protein.

Fig. 6a shows the frequency and dissipation changes upon adsorption of BSA on a non annealed PEM. In this case immediately after the assembly the PEM was exposed to the BSA solution. The frequency decreased meaning that there is adsorption of protein on top of the PEM. The frequency shift after deposition of the BSA was  $\Delta f = 186.5$  Hz. After rinsing with buffer the frequency increased with a total frequency shift of 102 Hz, proving the adsorption of the protein.

When BSA was deposited on the 37 °C annealed PEM the adsorption of the protein decreased to half compared with the non annealed PEM ( $\Delta f = 45.5$  Hz) (Fig. 6b). When the film is rinsed with the buffer there is a removal of non-bounded protein as the frequency increases to a higher value,  $\Delta f = 35$  Hz. In the case of annealing at 80 °C there is no apparent adsorption of protein (Fig. 6c). The total frequency shift after the BSA deposition was  $\Delta f = 3.5$  Hz. When the film is rinsed with buffer the frequency there is almost no change in frequency or dissipation indicating that there is no protein adsorption or deposition on the film annealed at 80 °C.

Advancing contact angle measurements on the films after deposition of the protein revealed a certain degree of hydrophobicity for all the cases. Nevertheless, for the case of adsorption of the BSA on non annealed PEMs we obtained the highest values 119° (Fig. 6a) while for the annealed samples at 37 and 80 °C the contact angle values were 93° and 89° respectively, which are close to the contact

angle values before annealing (Fig. 6b and c). This hints of a limited deposition of the BSA on the annealed PEMs.

In order to have additional information on the changes in protein adsorption to the film, fluorescently labeled BSA has been deposited on top of the PLL/Alg film and its fluorescence was quantified (Fig. 7). Results were in agreement with QCM-D measurements. There is a significant decrease in fluorescence from the non annealed to the annealed PEMs, meaning a lower amount of protein deposited. Normalizing the intensity curves to the non annealed PEM the intensity of the maxima of the curves for the annealed PEMs at 37 and 80 °C were 0.34 and 0.13 a.u. respectively, one third and one tenth of the values for the non annealed PEM.

QCM-D, contact angle, and fluorescence measurements show that thermal annealing has an impact on the interaction of BSA with the PEM. The change in hydrophilic character of the PEM with the annealing and the exposure of the alginate chains to the surface with compensated charges brings an antifouling character to the PEM. The decrease of protein adsorption with increasing temperature may be indicative of a more significant presence of alginate chains with compensated charges on the surface. It is known that alginate has an antifouling character that probably is increased if the charges of the alginate are partially neutralized [31,38]. The presence of a negative charge on the surface could also be responsible for the decrease on protein deposition as BSA preferentially adsorb on positively charged surfaces [35]. Further experiments on the study of the rearrangement of polyelectrolyte and the interaction with proteins are being performed.

## 4. Conclusions

We have shown that annealing of PLL/Alg PEMs at temperatures between 37 and 80 °C results in the film reorganization that could be interpreted as a change from stratified polyelectrolyte layers to the formation of complexes between the oppositely charged polyelectrolytes. Surface topography and charge change after annealing. Most interesting is that annealing has a clear impact on the wet-

ting properties of PEMs, whose contact angle changes from 36° to values between 77° and 95°. Surface energy calculations show that the annealing affects the polar energy of the surface, hinting a large compensation of charges after annealing at 37 and 80 °C. Our results show a simple way to change the wetting properties of surfaces from hydrophilic to hydrophobic without further chemical modifications. Results also show that annealing decreases protein deposition on the films. In conclusion, this work shows a simple way of tuning the wetting and antifouling character of biocompatible films that can be used for biomedical applications where low protein deposition is required.

## Acknowledgements

This work was financially supported by the Marie Curie project “Higraphen Hierarchical functionalization and assembly of Graphene for multiple device fabrication” (HiGRAPHEN) (Grant ref: 612704). The authors also acknowledge the project MAT2013-48169-R from the Spanish Ministry of Economy (MINECO). O.A. acknowledges financial support from ANPCyT (PICT 2010-2554 and PICT-2013-0905), Consejo Nacional de Investigaciones Científicas y Técnicas (CONICET) (PIP 11220130100370CO), Fundación Petruzza and the Austrian Institute of Technology GmbH (AIT-CONICET Partner Lab: “Exploratory Research for Advanced Technologies in Supramolecular Materials Science” – Exp. 4947/11, Res. No. 3911). M.A.P and O.A. are staff members of CONICET.

## Appendix A. Supplementary data

Supplementary data associated with this article can be found, in the online version, at <http://dx.doi.org/10.1016/j.colsurfb.2016.05.013>.

## References

- [1] G. Decher, M. Ecker, J. Schmitt, B. Struth, Layer-by-layer assembled multicomposite films, *Curr. Opin. Colloid Interface Sci.* 3 (1998) 32–39, [http://dx.doi.org/10.1016/S1359-0294\(98\)80039-3](http://dx.doi.org/10.1016/S1359-0294(98)80039-3).
- [2] C.J. Detzel, A.L. Larkin, P. Rajagopalan, Polyelectrolyte multilayers in tissue engineering, *Tissue Eng. Part B Rev.* 17 (2011) 101–113, <http://dx.doi.org/10.1089/ten.TEB.2010.0548>.
- [3] H.M.C. Gao, E. Donath, S. Moya, V. Dudnik, Elasticity of hollow polyelectrolyte capsules prepared by the layer-by-layer technique, *Eur. Phys. J. E* 5 (2001) 21–27.
- [4] A. Wu, D. Yoo, J.K. Lee, M.F. Rubner, Solid-state light-emitting devices based on the tris-chelated ruthenium(II) complex: 3. High efficiency devices via a layer-by-layer molecular-level blending approach, *J. Am. Chem. Soc.* 121 (1999) 4883–4891, <http://dx.doi.org/10.1021/ja9833624>.
- [5] L. Ouyang, R. Malaisamy, M.L. Bruening, Multilayer polyelectrolyte films as nanofiltration membranes for separating monovalent and divalent cations, *J. Memb. Sci.* 310 (2008) 76–84, <http://dx.doi.org/10.1016/j.memsci.2007.10.031>.
- [6] O. Onitsuka, A. C. Fou, M. Ferreira, B.R. Hsieh, M.F. Rubner, Enhancement of light emitting diodes based on self-assembled heterostructures of poly(p-phenylene vinylene), *J. Appl. Phys.* 80 (1996) 4067–4071, <http://dx.doi.org/10.1063/1.363369>.
- [7] I.F. Patel, M.V. Kiryukhin, N.L. Yakovlev, H.S. Gupta, G.B. Sukhorukov, Naturally inspired polyelectrolyte multilayer composite films synthesized through layer-by-layer assembly and chemically infiltrated with CaCO<sub>3</sub>, *J. Mater. Chem. B* 3 (2015) 4821–4830, <http://dx.doi.org/10.1039/C5TB00055F>.
- [8] C. Holmes, J. Daoud, P.O. Bagnaninchi, M. Tabrizian, Polyelectrolyte multilayer coating of 3D scaffolds enhances tissue growth and gene delivery: non-invasive and label-free assessment, *Adv. Healthc. Mater.* 3 (2014) 572–580, <http://dx.doi.org/10.1002/adhm.201300301>.
- [9] X. Zhu, D. Jańczewski, S.S.C. Lee, S.L.M. Teo, G.J. Vancso, Cross-linked polyelectrolyte multilayers for marine antifouling applications, *ACS Appl. Mater. Interfaces* 5 (2013) 5961–5968, <http://dx.doi.org/10.1021/am4015549>.
- [10] X. Zhu, S. Guo, D. Jańczewski, F.J. Parra Velandia, S.L.-M.M. Teo, G.J. Vancso, Multilayers of fluorinated amphiphilic polyions for marine fouling prevention, *Langmuir* 30 (2013) 288–296, <http://dx.doi.org/10.1021/la404300r>.
- [11] X. Zhu, D. Jańczewski, S. Guo, S.S.C. Lee, F.J. Parra Velandia, S.L. Teo, et al., Polyion multilayers with precise surface charge control for antifouling, *ACS Appl. Mater. Interfaces* 7 (2015) 852–861, <http://dx.doi.org/10.1021/am507371a>.
- [12] J. Irigoyen, N. Politakos, R. Murray, S.E. Moya, Design and fabrication of regenerable polyelectrolyte multilayers for applications in foulant removal, *Macromol. Chem. Phys.* 215 (2014) 1543–1550, <http://dx.doi.org/10.1002/macp.201400138>.
- [13] G. Decher, J.D. Hong, J. Schmitt, Buildup of ultrathin multilayer films by a self-assembly process: III. Consecutively alternating adsorption of anionic and cationic polyelectrolytes on charged surfaces, *Thin Solid Films* 210–211 (1992) 831–835, [http://dx.doi.org/10.1016/0040-6090\(92\)90417-A](http://dx.doi.org/10.1016/0040-6090(92)90417-A).
- [14] T.R. Farhat, J.B. Schlenoff, Ion transport and equilibria in polyelectrolyte multilayers, *Langmuir* 17 (2001) 1184–1192, <http://dx.doi.org/10.1021/la001298+>.
- [15] J.B. Schlenoff, H. Ly, M. Li, Charge and mass balance in polyelectrolyte multilayers, *J. Am. Chem. Soc.* 120 (1998) 7626–7634, <http://dx.doi.org/10.1021/ja980350+>.
- [16] R. Georgieva, S.E. Moya, H. Bäuml, H. Möhwald, E. Donath, Controlling ionic conductivity in lipid polyelectrolyte composite capsules by cholesterol, *J. Phys. Chem. B* 109 (2005) 18025–18030, <http://dx.doi.org/10.1021/jp0521407>.
- [17] T. Krebs, H.L. Tan, G. Andersson, H. Morgner, P. Gregory Van Patten, Increased layer interdiffusion in polyelectrolyte films upon annealing in water and aqueous salt solutions, *Phys. Chem. Chem. Phys.* 8 (2006) 5462–5468, <http://dx.doi.org/10.1039/b609440f>.
- [18] S.S. Shiratori, M.F. Rubner, pH-dependent thickness behavior of sequentially adsorbed layers of weak polyelectrolytes, *Macromolecules* 33 (2000) 4213–4219, <http://dx.doi.org/10.1021/ma991645q>.
- [19] D. Gregurec, M. Olszyna, N. Politakos, L. Yate, L. Dahne, S.E. Moya, Stability of polyelectrolyte multilayers in oxidizing media: a critical issue for the development of multilayer based membranes for nanofiltration, *Colloid Polym. Sci.* 293 (2014) 381–388, <http://dx.doi.org/10.1007/s00396-014-3423-5>.
- [20] G. Decher, J. Schmitt, Fine-Tuning of the film thickness of ultrathin multilayer films composed of consecutively alternating layers of anionic and cationic polyelectrolytes, *Prog. Colloid Polym. Sci.* 89 (1992) 160–164, <http://dx.doi.org/10.1007/BFb0116302>.
- [21] K. Köhler, D.G. Shchukin, H. Möhwald, G.B. Sukhorukov, Thermal behavior of polyelectrolyte multilayer microcapsules. 1. The effect of odd and even layer number, *J. Phys. Chem. B* 109 (2005) 18250–18259, <http://dx.doi.org/10.1021/jp052208i>.
- [22] C. Gao, S. Leporatti, S. Moya, E. Donath, H. Möhwald, Swelling and shrinking of polyelectrolyte microcapsules in response to changes in temperature and ionic strength, *Chem.—Eur. J.* 9 (2003) 915–920, <http://dx.doi.org/10.1002/chem.200390113>.
- [23] K. Köhler, D.G. Shchukin, G.B. Sukhorukov, H. Möhwald, Drastic morphological modification of polyelectrolyte microcapsules induced by high temperature, *Macromolecules* 37 (2004) 9546–9550, <http://dx.doi.org/10.1021/ma048474w>.
- [24] S. Leporatti, C. Gao, a Voigt, E. Donath, H. Möhwald, Shrinking of ultrathin polyelectrolyte multilayer capsules upon annealing: a confocal laser scanning microscopy and scanning force microscopy study, *Eur. Phys. J. E* 5 (2001) 13–20, <http://dx.doi.org/10.1007/s101890170082>.
- [25] K. Glinel, C. Déjournat, M. Prevot, B. Schöler, M. Schönhoff, R.V. Klitzing, Responsive polyelectrolyte multilayers, *Colloids Surf. A Physicochem. Eng. Asp.* 303 (2007) 3–13, <http://dx.doi.org/10.1016/j.colsurfa.2007.02.052>.
- [26] C. Picart, J. Mutterer, L. Richert, Y. Luo, G.D. Prestwich, P. Schaaf, et al., Molecular basis for the explanation of the exponential growth of polyelectrolyte multilayers, *Proc. Natl. Acad. Sci. U. S. A.* 99 (2002) 12531–12535, <http://dx.doi.org/10.1073/pnas.202486099>.
- [27] S.G. Caridade, C. Monge, F. Gilde, T. Boudou, J.F. Mano, C. Picart, Free-standing polyelectrolyte membranes made of chitosan and alginate, *Biomacromolecules* 14 (2013) 1653–1660, <http://dx.doi.org/10.1021/bm400314s>.
- [28] D.L. Elbert, C.B. Herbert, J.A. Hubbell, Thin polymer layers formed by polyelectrolyte multilayer techniques on biological surfaces, *Langmuir* 15 (1999) 5355–5362, <http://dx.doi.org/10.1021/la9815749>.
- [29] V. Krikorian, M. Kurian, M.E. Galvin, A.P. Nowak, T.J. Deming, D.J. Pochan, Polypeptide-based nanocomposite: structure and properties of poly(L-lysine)/Na<sup>+</sup>-montmorillonite, *J. Polym. Sci. Part B Polym. Phys.* 40 (2002) 2579–2586, <http://dx.doi.org/10.1002/polb.10315>.
- [30] R. Aston, M. Wimalaratne, A. Bröck, G. Lawrie, L. Grøndahl, Interactions between chitosan and alginate dialdehyde biopolymers and their layer-by-layer assemblies, *Biomacromolecules* 16 (2015) 1807–1817, <http://dx.doi.org/10.1021/acs.biomac.5b00383>.
- [31] J. Zhou, G. Romero, E. Rojas, L. Ma, S. Moya, C. Gao, Layer by layer chitosan/alginate coatings on poly(lactide-co-glycolide) nanoparticles for antifouling protection and Folic acid binding to achieve selective cell targeting, *J. Colloid Interface Sci.* 345 (2010) 241–247, <http://dx.doi.org/10.1016/j.jcis.2010.02.004>.
- [32] M. Mu, T. Rieser, K. Lunkwitz, J. Meier-haack, Polyelectrolyte complex layers: a promising concept for anti-fouling coatings verified by in-situ ATR-FTIR spectroscopy, *Macromol. Rapid Commun.* 20 (1999) 607–611, [http://dx.doi.org/10.1002/\(SICI\)1521-3927\(19991201\)20:12<607:AID-MARC607>3.0.CO;2-Z](http://dx.doi.org/10.1002/(SICI)1521-3927(19991201)20:12<607:AID-MARC607>3.0.CO;2-Z).
- [33] L. Henke, N. Nagy, U.J. Krull, An AFM determination of the effects on surface roughness caused by cleaning of fused silica and glass substrates in the process of optical biosensor preparation, *Biosens. Bioelectron.* 17 (2002) 547–555, [http://dx.doi.org/10.1016/S0956-5663\(02\)00012-X](http://dx.doi.org/10.1016/S0956-5663(02)00012-X).

- [34] J.D. Andrade, L.M. Smith, D.E. Gregonis, The contact angle and interface energetics, in: *surf, Interfacial Asp. Biomed. Polym.* 1985 (2016) 249–292, <http://dx.doi.org/10.1007/978-1-4684-8610-0-7>.
- [35] D.K. Owens, R.C. Wendt, Estimation of the surface free energy of polymers, *J. Appl. Polym. Sci.* 13 (1969) 1741–1747, <http://dx.doi.org/10.1592/phco.30.10.1004>.
- [36] C.J. van Oss, *Interfacial Forces in Aqueous Media*, Second Edition, 1994. 10.1016/0032-5910(95)90005-5.
- [37] G. Beamson, D. Briggs, High resolution XPS of organic polymers: the scienta ESCA3000 database, *J. Chem. Educ.* 70 (1993) A25, <http://dx.doi.org/10.1021/ed070pA25.5>.
- [38] K. Zhao, X. Zhang, J. Wei, J. Li, X. Zhou, D. Liu, et al., Calcium alginate hydrogel filtration membrane with excellent anti-fouling property and controlled separation performance, *J. Memb. Sci.* 492 (2015) 536–546, <http://dx.doi.org/10.1016/j.memsci.2015.05.075>.